Applied Physics Letters ARTICLE scitation.org/journal/apl

Complex optical conductivity of Bi_2Se_3 thin film: Approaching two-dimensional limit

Cite as: Appl. Phys. Lett. **118**, 191101 (2021); doi: 10.1063/5.0049170
Submitted: 2 March 2021 · Accepted: 25 April 2021 ·
Published Online: 10 May 2021

View Online Export Citation CrossMark

Mingsheng Fang,[1] Zhenyu Wang,[2,3] Honggang Gu,[1,a)] Baokun Song,[1] Zhengfeng Guo,[1] Jinlong Zhu,[1] Xiuguo Chen,[1] Chuanwei Zhang,[1] Hao Jiang,[1] and Shiyuan Liu[1,a)]

AFFILIATIONS

[1]State Key Laboratory of Digital Manufacturing Equipment and Technology, Huazhong University of Science and Technology, Wuhan 430074, China
[2]National Innovation Institute of Defense Technology, Academy of Military Sciences PLA China, Beijing 100010, People's Republic of China
[3]Beijing Academy of Quantum Information Sciences, Beijing 100084, People's Republic of China

[a)]**Authors to whom correspondence should be addressed:** hongganggu@hust.edu.cn and shyliu@hust.edu.cn

ABSTRACT

Two-dimensional Bi_2Se_3 thin films have attracted widespread attention as an ideal platform of high-performance optoelectronic applications. Understanding the intrinsic optical/electronic properties of Bi_2Se_3 thin films is vital for Bi_2Se_3-based optoelectronic applications. Here, the complex optical conductivities of a series of Bi_2Se_3 thin films with a varying number of quintuple layers are investigated by combining spectroscopic ellipsometry with the classical slab model over a broad spectral range of 0.73–6.43 eV. Results show that the zero-cross point of the imaginary complex optical conductivity exhibits a blueshift trend due to the enhanced coupling between the surface states as the thickness of Bi_2Se_3 thin film approaches the two-dimensional limit. Five feature peaks (A–E) are identified in the complex optical conductivity spectra, and their center energies exhibit interesting thickness dependencies, which are mainly attributed to the increased surface state gap due to the finite-size effects when the Bi_2Se_3 thin film gradually approaches the two-dimensional limit. Our work not only gives insights into the tunable optical properties of Bi_2Se_3 thin films but also reveals its intrinsic physical origin, which are essential and imperative for accurate modeling and design of Bi_2Se_3-based optoelectronic devices.

Topological insulator (TI) materials, such as HgCdTe quantum wells, Bi_2Te_3, Bi_2Se_3, Sb_2Te_3, etc., have gained great interest in many fields, including quantum computers, condensed-matter physics, optoelectronics, and magnetism.[1–5] Unlike normal insulators, the TIs not only have a narrow bulk bandgap induced by the strong spin–orbit coupling but also possess gapless and dissipationless spin-polarized edge or surface states.[6–8] In three-dimensional (3D) TIs, the Dirac cones, spin-polarized surface states, and electronic band structures were observed and obtained by employing angle-resolved photoemission spectroscopy (ARPES), spin-resolved ARPES, and first principle calculations, which demonstrate the topological nature of 3D TIs.[1,9,10] Among various 3D TIs, the Bi_2Se_3 is the most representative one, which has been extensively applied into many optoelectronic devices.[11–13] Bi_2Se_3 possesses a layered structure composed of quintuple layers (QLs) with weak van der Waals-type interaction among adjacent QLs, which makes it available to obtain Bi_2Se_3 thin films. Among all the growth methods, molecular beam epitaxy (MBE) is a widely used approach to fabricate high-quality Bi_2Se_3 thin films.[14,15] As the thickness of Bi_2Se_3 approaches a few QLs, the performance of Bi_2Se_3-based optoelectronic devices can be dramatically enhanced with a widely tunable surface bandgap.[16] To provide a guidance for the design and optimization of optoelectronic devices based on Bi_2Se_3 thin films, it is critical to obtain accurate and quantitative characterization of the optical properties of Bi_2Se_3 thin films.

Generally speaking, the complex refractive index and the complex dielectric function are two basic optical functions that we regularly use to, respectively, describe the optical and dielectric properties of a material. Except for them, the complex optical conductivity, as another essential optical function, is directly relevant to the photoresistance and photocurrent, which is beneficial to the development of related optoelectronic devices, including photodetectors, photoconductors, photovoltaics, etc.[17–19] Therefore, the complex optical

conductivities of Bi_2Se_3 have been extensively studied by multiple approaches, such as reflection spectrometry, UV-visible ellipsometry, terahertz spectroscopy, and first-principles calculations.[20–25] Pietro *et al.* measured the reflectance spectrum of Bi_2Se_3 single crystal from sub-THZ to the visible region in the range of 5–300 K and calculated the real part of complex optical conductivity via the reflectivity by Kramers–Kronig transformations.[21] Post *et al.* obtained the infrared complex optical conductivities of Bi_2Se_3 films with a thickness varying from 15 QLs to 99 QLs by spectroscopic ellipsometry (SE) and infrared transmission spectroscopy.[22] By measuring the THz transmittance vs the temperature of 23-QL Bi_2Se_3 film, Kamboj *et al.* extracted the THz optical conductance spectra from the normalized transmission using Tinkham's formula.[23] On the other hand, some researchers focused on using different theoretical methods to predict the complex optical conductivity of Bi_2Se_3 crystal by density functional theory (DFT).[24,25] However, most of the aforementioned works focus on the investigation of the complex optical conductivity of Bi_2Se_3 over a narrow band and are limited to the thick Bi_2Se_3 films or single crystal. The systematic research on the complex optical conductivity of Bi_2Se_3 at the two-dimensional limit (<6 QLs)[26] is missing, which may hinder the performance improvement of Bi_2Se_3-based optoelectronic devices.

In this work, high-quality and continuous Bi_2Se_3 thin films with variable thickness are prepared by MBE on sapphire substrate. We have systematically investigated the complex optical conductivities of the as-prepared Bi_2Se_3 thin films as a function of the number of QL by combining spectroscopic ellipsometry (SE) with the classical slab model. Five feature peaks (A–E) are observed in the complex optical conductivity spectra. Our studies reveal that the zero-cross point of the imaginary part of the complex optical conductivity shows a blue-shift trend due to enhanced coupling between the opposite surfaces as the thickness gradually decreases. By using differential spectrum analysis method, we accurately determine the center energies of feature peaks in the optical conductivity spectra and reveal the intriguing thickness dependencies of their center energies. Results suggest that the increased surface state gap due to the finite-size effect mainly leads to the layer-dependent evolutions of these feature peaks.

High-quality and continuous Bi_2Se_3 thin films were prepared by the MBE on the sapphire (Al_2O_3) substrate.[27,28] The detailed growth process was demonstrated in the supplementary material. After the growth of Bi_2Se_3 thin films, several characterization methods were applied to demonstrate the high quality of our MBE-grown Bi_2Se_3 thin film samples. The RH30OM reflection high-energy electric diffraction (RHEED) system and Raman spectrometer (inVia reflex, RENISHAW) were adopted to detect the crystal quality of Bi_2Se_3 thin films. The optical microscope (OM) measurements were conducted with a 10 times magnification to check the surface conditions of Bi_2Se_3 thin films, and the thicknesses and surface roughness of Bi_2Se_3 thin films were examined by an AFM system (Bruker Dimension Icon) and a high-resolution transmission electron microscope (HRTEM) system (FEI Tian G2–300).

The ellipsometric data were gathered using a commercial dual rotating-compensator spectroscopic ellipsometer (ME-L Muller matrix ellipsometer, Wuhan Eoptics Technology Corporation). Optical spectra of Bi_2Se_3 thin films were recorded over an ultra-broad spectral

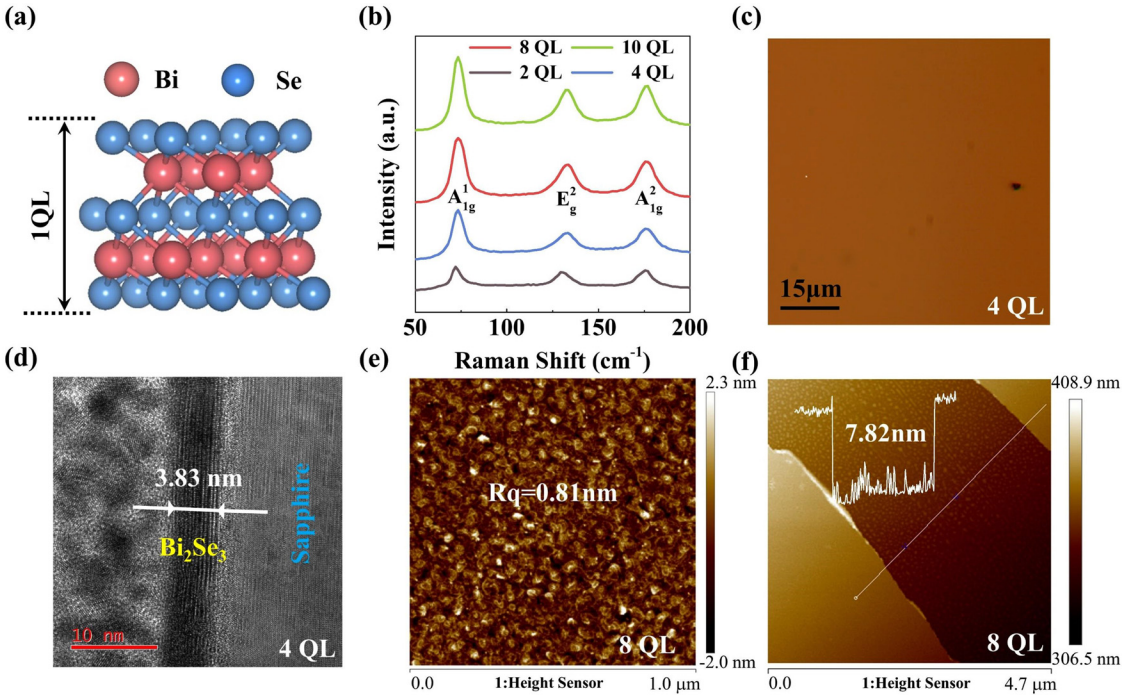

FIG. 1. (a) The schematic diagram of Bi_2Se_3; five atomic layers of Se1–Bi–Se2–Bi–Se1 form a QL. (b) Raman spectra of 2-QL, 4-QL, 8-QL, and 10-QL Bi_2Se_3 thin films. (c) Representative OM graph of the 4-QL Bi_2Se_3 thin film. (d) Cross-sectional HRTEM image of 4-QL Bi_2Se_3 thin film. (e) and (f) The surface roughness and thickness of 8-QL Bi_2Se_3 thin film characterized by AFM.

range of 0.73–6.43 eV. A pair of focusing probes was used in the measuring process, and the diameter of the probing spot can be as small as 200 μm. The multi-incidence measurement mode was used to reduce the correlations among the variables, and the incident angles for each sample were set from 60° to 70° with a step of 5°.

The Bi_2Se_3 thin film possesses a rhombohedral crystal structure, and it belongs to the space group $R\bar{3}m$.[29] As denoted in Fig. 1(a), from the top to the bottom atomic layers in a QL, the Se and Bi atoms are stacked on the order of Se1–Bi–Se2–Bi–Se1. The purity and crystal quality of Bi_2Se_3 thin films are checked by Raman spectra, as presented in Fig. 1(b). The Raman spectra show that the Bi_2Se_3 thin films possess three characteristic intensity peaks (A^1_{1g}, E^2_g, and A^2_{1g}) around 73.4, 131.5, and 174.5 cm^{-1}, respectively, suggesting the high purity and crystal quality of our Bi_2Se_3 thin film samples.[28,30] The typical RHEED pattern of Bi_2Se_3 is presented in Ref. 31, indicating the lattice constant of Bi_2Se_3 is 4.194 Å. The smooth surface shown in the OM image in Fig. 1(c) indicates that our Bi_2Se_3 samples are flat and continuous. Besides, as shown in Fig. 1(d), the thickness of the 4-QL Bi_2Se_3 thin film is determined by the HRTEM, and it is 3.83 nm. The clear layered structures shown in the HRTEM image indicate the high crystalline quality of the Bi_2Se_3 thin film. Figures 1(e) and 1(f) present the surface condition and thickness of 8-QL Bi_2Se_3 thin film detected by AFM. It is clear that the roughness values (*Rq*) of film are extremely low, demonstrating the Bi_2Se_3 thin film has great flatness. The AFM image also shows that the thickness of 8-QL Bi_2Se_3 thin film is 7.82 nm. All these characterizations show that the Bi_2Se_3 thin films in our study are high quality and continuous.

Figures 2(a) and 2(b) show the complex refractive indices $N = n - i\kappa$ extracted from ellipsometric analysis processes (detailed analysis processes are demonstrated in the supplementary material), where n and κ represent the refractive index and the extinction coefficient, respectively. Up to five absorption peaks (A–E) can be observed in the complex refractive index spectra of 2–10 QL Bi_2Se_3 thin films. As the thickness of Bi_2Se_3 thin films decreases from 10 QLs to six QLs, both the magnitudes of n and κ remain nearly unchanged. While the thickness becomes thinner than six QLs, the evolution trends of the magnitudes are different for n and κ. Figure 2(a) shows that with the thickness decreasing, the magnitude of n gradually decreases in the energy range from 0.73 to 2.2 eV, but it turns to gradually increases when the photon energy is greater than 2.2 eV. Different from n, Fig. 2(b) shows that with the thickness decreasing, the magnitude of κ gradually decreases in the energy range from 0.73 to 4.5 eV. Additionally, the energy positions of these five absorption peaks (A–E) present blueshift trends as the thickness approaches the two-dimensional limit. The spectral shape of Bi_2Se_3 thin films in Figs. 2(a) and 2(b) is similar to that of few-layer black phosphorus and tellurium, and their optical respond is sensitive to thickness.[32,33] Previous studies[32,33] on few-layer black phosphorus and tellurium are focused on infrared range and anisotropy, while our study on Bi_2Se_3 thin films is on a wide range and isotropic, similar to normal 2D transition metal dichalcogenides (TMDCs).[34]

Base on the complex refractive index, the complex optical conductivities $\sigma = \sigma_r + i\sigma_i$ of Bi_2Se_3 thin films can be evaluated by the classical slab model. In the classical slab model, the thin film is

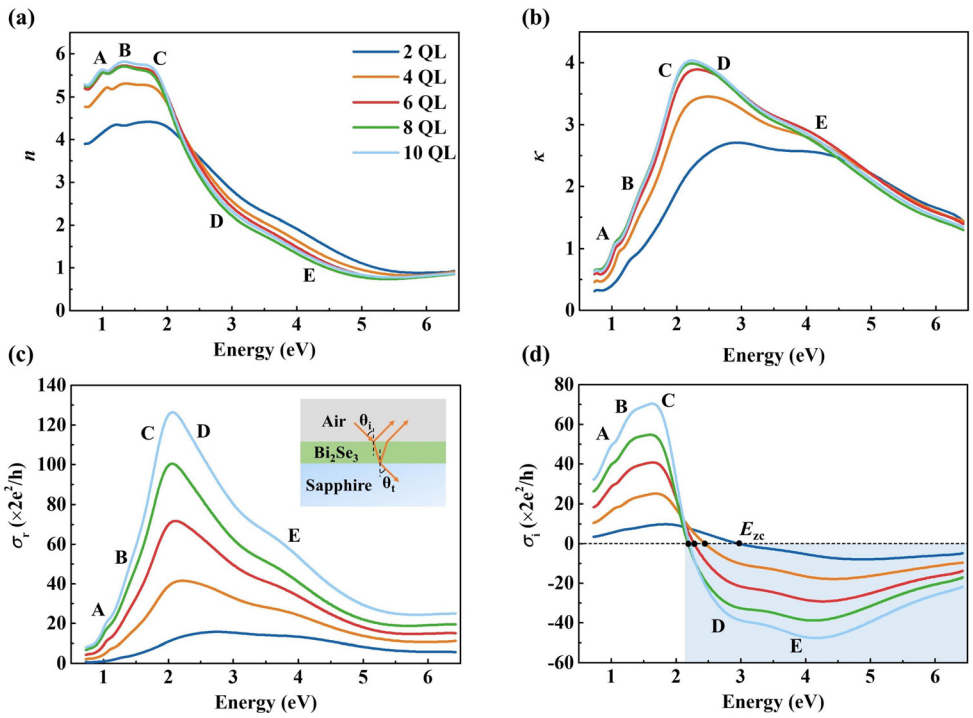

FIG. 2. Complex refractive index spectra and complex optical conductivity spectra of 2–10 QL Bi_2Se_3 thin films. (a) Refractive index n. (b) Extinction coefficient κ. (c) Real part of complex optical conductivity σ_r; the inset shows the classical slab model. (d) Imaginary part of complex optical conductivity σ_i; the blue area demonstrates the negative σ_i zone. Five absorption peaks are labeled with A–E.

considered as a slab with a finite thickness (d), and the complex optical conductivities can be calculated by[17]

$$\sigma = \sigma_r + i\sigma_i = id\varepsilon_0\omega(N^2 - 1), \quad (1)$$

where d is the thickness of the Bi_2Se_3 thin film determined by SE (Table S1), N is the complex refractive index shown in Figs. 2(a) and 2(b), ε_0 and ω refer to the free-space permittivity and the angular frequency of light, respectively. Figures 2(c) and 2(d) present the complex optical conductivities of 2–10 QL Bi_2Se_3 thin films evaluated by the classical slab model, which have been normalized by $2e^2/h$ (e and h represent the electronic charge and Plank constant). Similar to the complex refractive index, five feature peaks are also observed in the complex optical conductivity spectra. In the real complex optical conductivity (σ_r), it is obvious that σ_r monotonically decreases as the thickness of Bi_2Se_3 thin film approaches the two-dimensional limit, and in the imaginary complex optical conductivity (σ_i), the absolute value of σ_i also shows a decrease trend as the thickness of Bi_2Se_3 thin film gradually decreases. These decrease trends in the real and imaginary parts of complex optical conductivity can be attributed to the gradually attenuated light absorption and propagation effects with the thickness decreasing. In addition, it can be observed that there exists a region highlighted by the blue area in Fig. 2(d), where the σ_i becomes negative. This negative phenomenon is related to the surface plasma and expected to present some novel insights for the design of Bi_2Se_3-based devices, such as plasmon-based radiation generation, sensing, and waveguides.[16,21,35,36] Specifically, as the thickness of Bi_2Se_3 thin film approaches the two-dimensional limit, the zero-cross point (E_{zc}) shows a blueshift trend, and the area where σ_i is negative gradually becomes smaller in Fig. 2(d). We propose that when the Bi_2Se_3 thin film is getting thinner, the enhanced coupling between the opposite surface states causes an increase in surface state gap,[26,27] and then makes the resonance frequencies of surface plasma increase, which finally lead to the blueshifted E_{zc} and the shrunken negative σ_i area.

As presented in Fig. 2, except for that the magnitudes of feature peaks (A–E) in complex optical conductivity spectra demonstrate layer-dependencies; the center energies of these peaks also exhibit interesting layer-dependent shifts. In order to accurately determine the center energies of these peaks and further reveal the underlying physical essence, we calculate the first-order and second-order differential spectra of the complex optical conductivities of Bi_2Se_3 thin films, as shown in Fig. 3. The feature peaks of complex optical conductivity

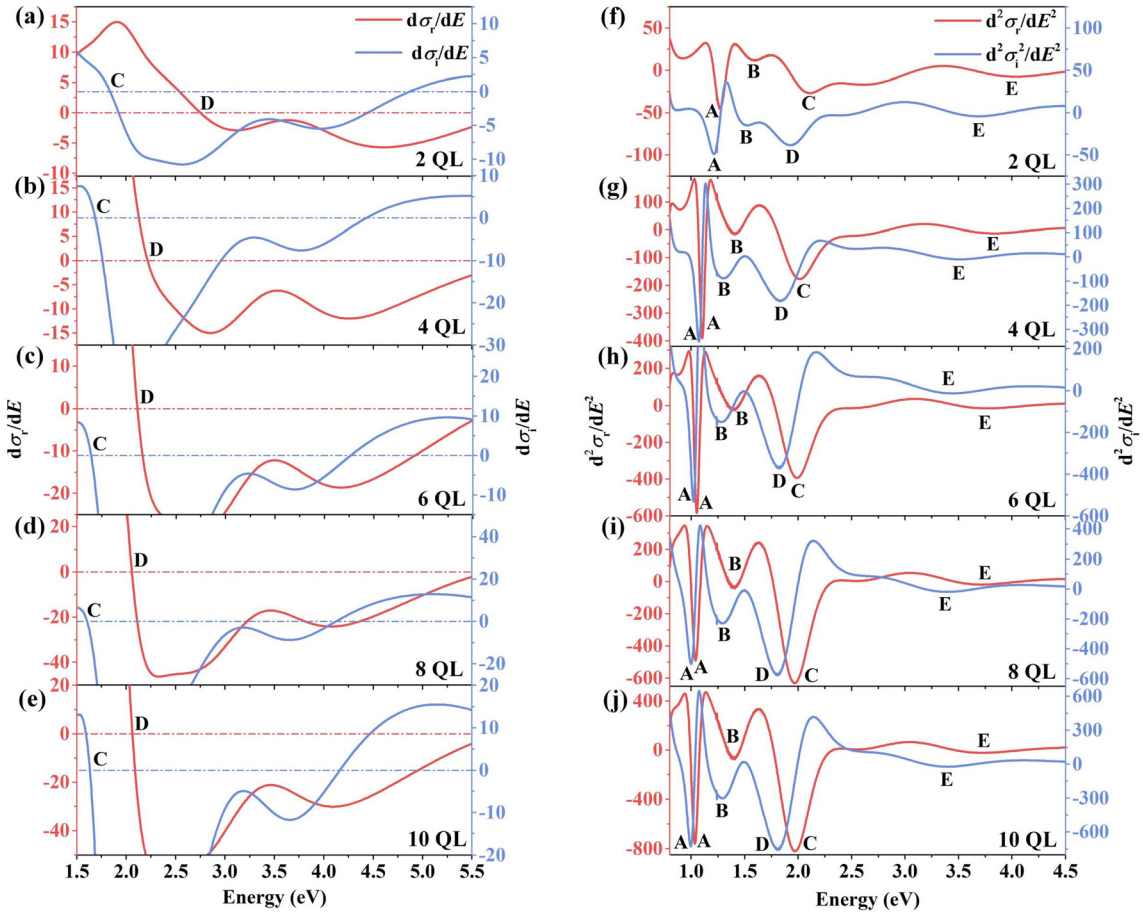

FIG. 3. Differential spectra of the complex optical conductivities of 2–10 QL Bi_2Se_3 thin films. (a)–(e) First-order differential spectra over the region of 1.5–5.5 eV. (f)–(j) Second-order differential spectra over the region of 1.0–4.5 eV. Five feature peaks are labeled with A–E.

spectra in Fig. 2 can be classified into extreme peaks and shoulder peaks. The center energies of extreme peaks are identical to the positive-to-negative zero-cross points in first-order differential spectra, and the center energies of shoulder peaks are equivalent to the local minima of the second-order differential spectra. The red (blue) solid lines in Figs. 3(a)–3(e) show the first-order differential spectra of the real (imaginary) parts of the complex optical conductivities of 2–10 QL Bi_2Se_3 thin films. The extreme peak D in σ_r and extreme peak C in σ_i are accurately identified at the positive-to-negative zero-cross point in Figs. 3(a)–3(e). Apart from extreme peak D in σ_r and extreme peak C in σ_i, other feature peaks are shoulder peaks and can be identified at the local minima in the second-order differential spectra of σ, as shown in Figs. 3(f)–3(j). The center energies of the feature peaks (A–E) in the real and imaginary part of complex optical conductivity spectra are listed in Tables S2 and S3.

Figures 4(a) and 4(b) present the layer-dependent evolutions of the center energies of the feature peaks A–E in the complex optical conductivity spectra. The E_0^{Re} in Fig. 4(a) and the E_0^{Im} in Fig. 4(b) illustrate the center energies of feature peaks A–E in the real and imaginary part of the complex optical conductivity spectra, respectively. In the real complex optical conductivity spectra E_0^{Re}, when the QL number of Bi_2Se_3 thin film decreases from 10 to 6, the center energies of feature peaks A–E remain nearly unchanged. As the QL number of Bi_2Se_3 thin film continues to decrease, the center energies of feature peak A–E show a blueshift trend. Among these five feature peaks, the feature peak D shows a maximum blue shift of 0.64 eV, while the feature peak C shows a minimum blue shift of 0.13 eV. Previous work[37] shows that electron energy-loss spectroscopy (EELS) spectrum of Bi_2Se_3 bulk system has two main spectral features near 7 and 17 eV, and the spectral feature near 7 eV is related to pi plasmon resonances, similar to the pi plasmon in carbon nanotubes.[38] So, feature peaks A–E in Fig. 4(a) should be normal absorption peaks. In the imaginary optical conductivity spectra E_0^{Im}, as the thickness of Bi_2Se_3 thin film decreases from 10 QLs to six QLs, the center energy of feature peak C has some fluctuations, while the center energies of other feature peaks remain nearly the same. When the QL number of Bi_2Se_3 thin film is less than six QL, the center energies of all these five feature peaks A–E also present a blueshift trend. In addition, as the thickness of Bi_2Se_3 thin films

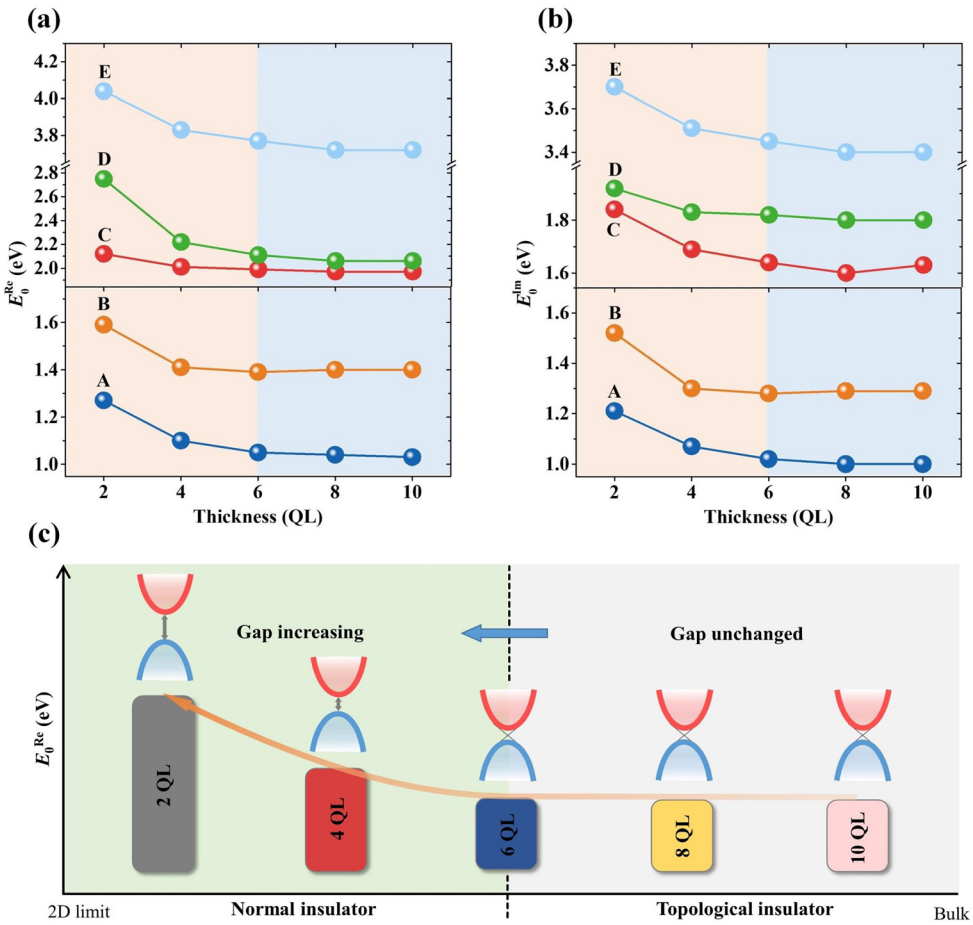

FIG. 4. (a) and (b) Center energies of feature peaks A–E in the real and imaginary part of complex optical conductivity spectra vs the QL number of Bi_2Se_3 thin films. (c) Schematic diagram of the evolution mechanism in E_0^{Re} as the thickness approaches the two-dimensional limit.

approaches two-dimensional limit, the feature peaks C and D gradually move away from each other in E_0^{Re}, but the feature peaks C and D are gradually approaching each other in E_0^{Im}.

Generally speaking, the real part of complex optical conductivity (σ_r) shows the energy loss component caused by the light-induced conduction current, while the imaginary part of complex optical conductivity (σ_i) can reflect the energy storage capacity of Bi_2Se_3 thin films. So, the feature peaks A–E in E_0^{Re} actually reflect energy loss in the light propagation process and should be related to different optical transitions. First-principles study in Ref. 24 demonstrates that weak excitonic effects exist in optical properties of Bi_2Se_3, indicating the feature peaks A–E in E_0^{Re} have excitonic character. Besides, the feature peaks A–E are relevant to different direct transitions from valence bands to conduct bands along the Γ–M–K branch in the band structures of the Bi_2Se_3 thin films, as discussed in detail in previous work.[31,39] In 2D MoS_2 and 2D WSe_2, as the thickness decreases from multi-layers to monolayer, most of the energy shift values of feature peaks are below 0.2 eV, and high-energy feature peaks have a different trend from low-energy feature peaks. The underlying physical cause is explained as the alternate domination of the layer-dependent increasing exciton binding energy and the band renormalization.[17,40] Compared with 2D MoS_2 and 2D WSe_2, we elucidate that the excitonic effect is weak in Bi_2Se_3 thin films, and there are two factors that mainly affect the distinctive QL-dependent shifts in E_0^{Re}: one factor is the band shape evolution and the other is the increasing surface bandgap when the Bi_2Se_3 thin film varies from six QLs to two QLs. As shown in Fig. 4(c), the Bi_2Se_3 thin film experiences a dimensional crossover from 3D topological insulator to trivial insulator at six QLs,[26,27,31,39] which means as the QL number of Bi_2Se_3 thin film is less than six QLs, a finite bandgap opens in the surface states of the Bi_2Se_3 thin film due to the finite-size effects. We think that the fluctuations of A–E from 10 QLs to six QLs and the different blueshift values (0.13 eV–0.64 eV) of A–E below six QL could be attributed to band shape evolution as the thickness of Bi_2Se_3 thin film approaches two-dimensional limits, and the overall blueshift tendency is mainly caused by the increased surface state gap due to the finite-size effects when the QL decreases from 6 to 2.

In summary, we have provided systematic investigation of the QL-dependent optical conductivities of Bi_2Se_3 thin films by combining SE with the classical slab model. Five feature peaks (A–E) can be identified in the complex optical conductivity spectra, and the zero-cross point of the imaginary complex optical conductivity shows a blueshift trend due to enhanced coupling between the opposite surfaces as the thickness of Bi_2Se_3 thin film approaches the two-dimensional limit. With the help of differential spectrum analysis method, we determined the center energies of A–E in the optical conductivity spectra, whose center energies exhibit intriguing thickness dependencies. As the QL number of Bi_2Se_3 thin film decreases from ten to six, the center energies of A–E remain almost unchanged. While the QL number continues to decrease, the center energies of A–E present a blueshift trend as the QL number decreases. We attribute this evolution mainly to the increased surface state gap caused by the finite-size effects as the thickness gradually decreases. We anticipate that the determined complex optical conductivity of Bi_2Se_3 alongside their layer-dependent properties may pave the route to the design and performance improvement of photodetectors, photoconductors, and photovoltaics.

See the supplementary material for the detailed MBE growth process and ellipsometric analysis, and the center energies of the feature peaks (A–E) in the real and imaginary part of complex optical conductivity spectra from differential spectrum analysis.

AUTHORS' CONTRIBUTIONS

M.F. and Z.W. contributed equally to this work.

This work was funded by the National Natural Science Foundation of China (Grant Nos. 51727809, 51805193, 51525502, and 12004434), the National Key Research and Development Plan (Grant No. 2017YFF0204705), the General Program of Beijing Academy of Quantum Information Sciences (Project No. Y18G17), the National Science and Technology Major Project of China (Grant No. 2017ZX02101006–004), and the Fundamental Research Funds for the Central Universities (Grant No. 2021XXJS113).

DATA AVAILABILITY

The data that support the findings of this study are available from the corresponding author upon reasonable request.

REFERENCES

[1]M. Z. Hasan and C. L. Kane, "Colloquium: Topological insulators," Rev. Mod. Phys. **82**, 3045–3067 (2010).
[2]C. Zhao, Y. Zou, Y. Chen, Z. Wang, S. Lu, H. Zhang, S. Wen, and D. Tang, "Wavelength-tunable picosecond soliton fiber laser with topological insulator: Bi_2Se_3 as a mode locker," Opt. Express **20**, 27888–27895 (2012).
[3]Y. Xu, I. Miotkowski, C. Liu, J. Tian, H. Nam, N. Alidoust, J. Hu, C.-K. Shih, M. Z. Hasan, and Y. P. Chen, "Observation of topological surface state quantum Hall effect in an intrinsic three-dimensional topological insulator," Nat. Phys. **10**, 956–963 (2014).
[4]J. Yao, Z. Zheng, and G. Yang, "All-layered 2D optoelectronics: A high-performance UV–vis–NIR broadband SnSe photodetector with Bi_2Te_3 topological insulator electrodes," Adv. Funct. Mater. **27**, 1701823 (2017).
[5]J. Wang, B. Lian, and S.-C. Zhang, "Electrically tunable magnetism in magnetic topological insulators," Phys. Rev. Lett. **115**, 036805 (2015).
[6]L. Fu and C. L. Kane, "Topological insulators with inversion symmetry," Phys. Rev. B **76**, 045302 (2007).
[7]M. König, S. Wiedmann, C. Brüne, A. Roth, H. Buhmann, L. W. Molenkamp, X.-L. Qi, and S.-C. Zhang, "Quantum spin Hall insulator state in HgTe quantum wells," Science **318**, 766–770 (2007).
[8]L. Fu, C. L. Kane, and E. L. Mele, "Topological insulators in three dimensions," Phys. Rev. Lett. **98**, 106803 (2007).
[9]D. Hsieh, Y. Xia, L. Wray, D. Qian, A. Pal, J. H. Dil, J. Osterwalder, F. Meier, G. Bihlmayer, C. L. Kane, Y. S. Hor, R. J. Cava, and M. Z. Hasan, "Observation of unconventional quantum spin textures in topological insulators," Science **323**, 919–922 (2009).
[10]Y. L. Chen, J.-H. Chu, J. G. Analytis, Z. K. Liu, K. Igarashi, H.-H. Kuo, X. L. Qi, S. K. Mo, R. G. Moore, D. H. Lu, M. Hashimoto, T. Sasagawa, S. C. Zhang, I. R. Fisher, Z. Hussain, and Z. X. Shen, "Massive Dirac fermion on the surface of a magnetically doped topological insulator," Science **329**, 659–662 (2010).
[11]H. Zhang, X. Zhang, C. Liu, S.-T. Lee, and J. Jie, "High-responsivity, high-detectivity, ultrafast topological insulator Bi_2Se_3/silicon heterostructure broadband photodetectors," ACS Nano **10**, 5113–5122 (2016).
[12]M. Salvato, M. Scagliotti, M. D. Crescenzi, P. Castrucci, F. D. Matteis, M. Crivellari, S. P. Cresi, D. Catone, T. Bauch, and F. Lombardi, "Stoichiometric Bi_2Se_3 topological insulator ultrathin films obtained through a new fabrication process for optoelectronic applications," Nanoscale **12**, 12405 (2020).
[13]S. Wang, Y. Li, A. Ng, Q. Hu, Q. Zhou, X. Li, and H. Liu, "2D Bi_2Se_3 van der Waals epitaxy on mica for optoelectronics applications," Nanomaterials **10**, 1653 (2020).

[14]S.-K. Jerng, K. Joo, Y. Kim, S.-M. Yoon, J. H. Lee, M. Kim, J. S. Kim, E. Yoon, S.-H. Chuna, and Y. S. Kim, "Ordered growth of topological insulator Bi_2Se_3 thin films on dielectric amorphous SiO_2 by MBE," Nanoscale **5**, 10618 (2013).
[15]N. Bansal, Y. S. Kim, E. Edrey, M. Brahlek, Y. Horibe, K. Iida, M. Tanimura, G.-H. Li, T. Feng, H.-D. Lee, T. Gustafsson, E. Andrei, and S. Oh, "Epitaxial growth of topological insulator Bi_2Se_3 film on Si(111) with atomically sharp interface," Thin Solid Films **520**, 224–229 (2011).
[16]X. Zhang, J. Wang, and S.-C. Zhang, "Topological insulators for high-performance terahertz to infrared applications," Phys. Rev. B **82**, 245107 (2010).
[17]B. Song, H. Gu, M. Fang, Y.-T. Ho, X. Chen, H. Jiang, and S. Liu, "Complex optical conductivity of two-dimensional MoS_2: A striking layer dependency," J. Phys. Chem. Lett. **10**, 6246–6252 (2019).
[18]W.-C. Shen, R.-S. Chen, and Y.-S. Huang, "Photoconductivities in MoS_2 nanoflake photoconductors," Nanoscale Res. Lett. **11**, 124 (2016).
[19]F. H. L. Koppens, T. Mueller, P. Avouris, A. C. Ferrari, M. S. Vitiello, and M. Polini, "Photodetectors based on graphene, other two-dimensional materials and hybrid systems," Nat. Nanotechnol. **9**, 780–793 (2014).
[20]A. D. LaForge, A. Frenzel, B. C. Pursley, T. Lin, X. Liu, J. Shi, and D. N. Basov, "Optical characterization of Bi_2Se_3 in a magnetic field: Infrared evidence for magnetoelectric coupling in a topological insulator material," Phys. Rev. B **81**, 125120 (2010).
[21]P. D. Pietro, F. M. Vitucci, D. Nicoletti, L. Baldassarre, P. Calvani, R. Cava, Y. S. Hor, U. Schade, and S. Lupi, "Optical conductivity of bismuth-based topological insulators," Phys. Rev. B **86**, 045439 (2012).
[22]K. W. Post, B. C. Chapler, L. He, X. Kou, K. L. Wang, and D. N. Basov, "Thickness-dependent bulk electronic properties in Bi_2Se_3 thin films revealed by infrared spectroscopy," Phys. Rev. B **88**, 075121 (2013).
[23]V. S. Kamboj, A. Singh, T. Ferrus, H. E. Beere, L. B. Duffy, T. Hesjedal, C. H. W. Barnes, and D. A. Ritchie, "Probing the topological surface state in Bi_2Se_3 thin films using temperature-dependent terahertz spectroscopy," ACS Photonics **4**, 2711–2718 (2017).
[24]A. Lawal, A. Shaari, R. Ahmed, and N. Jarkoni, "First-principles many-body comparative study of Bi_2Se_3 crystal: A promising candidate for broadband photodetector," Phys. Lett. A **381**, 2993–2999 (2017).
[25]G. Tse and D. Yu, "The first principle study: Electronic and optical properties in Bi_2Se_3," Comput. Condens. Matter **4**, 59–63 (2015).
[26]Y. Zhang, K. He, C. Z. Chang, C. L. Song, L. L. Wang, X. Chen, J. F. Jia, Z. Fang, X. Dai, W. Y. Shan, S. Q. Shen, Q. Niu, X. L. Qi, S. C. Zhang, X. C. Ma, and Q. K. Xue, "Crossover of the three-dimensional topological insulator Bi_2Se_3 to the two-dimensional limit," Nat. Phys. **6**, 584–588 (2010).
[27]Z. Wang, T. Zhou, T. Jiang, H. Sun, Y. Zang, Y. Gong, J. Zhang, M. Tong, X. Xie, Q. Liu, C. Chen, K. He, and Q. K. Xue, "Dimensional crossover and topological nature of the thin films of a three-dimensional topological insulator by band gap engineering," Nano Lett. **19**, 4627–4633 (2019).
[28]J. Zhang, T. Jiang, T. Zhou, H. Ouyang, C. Zhang, Z. Xin, Z. Wang, and X. Cheng, "Saturated absorption of different layered Bi_2Se_3 films in the resonance zone," Photonics Res. **6**, C8–C14 (2018).
[29]R. Wyckoff, *Crystal Structures*, 2nd ed. (Interscience Publishers, 1963), pp. 1–44.
[30]J. Zhang, Z. Peng, A. Soni, Y. Zhao, Y. Xiong, B. Peng, J. Wang, M. S. Dresselhaus, and Q. Xiong, "Raman spectroscopy of few-quintuple layer topological insulator Bi_2Se_3 nanoplatelets," Nano Lett. **11**, 2407–2414 (2011).
[31]M. Fang, Z. Wang, H. Gu, M. Tong, B. Song, X. Xie, T. Zhou, X. Chen, H. Jiang, T. Jiang, and S. Liu, "Layer-dependent dielectric permittivity of topological insulator Bi_2Se_3 thin films," Appl. Surf. Sci. **509**, 144822 (2020).
[32]M. C. Sherrott, W. S. Whitney, D. Jariwala, S. Biswas, C. M. Went, J. Wong, G. R. Rossman, and H. A. Atwater, "Anisotropic quantum well electro-optics in few-layer black phosphorus," Nano Lett. **19**, 269–276 (2019).
[33]J. Qiao, Y. Pan, F. Yang, C. Wang, Y. Chai, and W. Ji, "Few-layer tellurium: One-dimensional-like layered elementary semiconductor with striking physical properties," Sci. Bull. **63**, 159–168 (2018).
[34]V. W. Brar, M. C. Sherrott, and D. Jariwala, "Emerging photonic architectures in two-dimensional opto-electronics," Chem. Soc. Rev. **47**, 6824 (2018).
[35]J. Yin, H. N. Krishnamoorthy, G. Adamo, A. M. Dubrovkin, Y. Chong, N. I. Zheludev, and C. Soci, "Plasmonics of topological insulators at optical frequencies," NGP Asia Mater. **9**, e425 (2017).
[36]X. Niu, X. Hu, S. Chu, and Q. Gong, "Epsilon-near-zero photonics: A new platform for integrated devices," Adv. Opt. Mater. **6**, 1701292 (2018).
[37]G. J. Shu, S. C. Liou, S. K. Karna, R. Sankar, M. Hayashi, and F. C. Chou, "Dynamic surface electronic reconstruction as symmetry-protected topological orders in topological insulator Bi_2Se_3," Phys. Rev. Mater. **2**, 044201 (2018).
[38]B. Song, F. Liu, H. Wang, J. Miao, Y. Chen, P. Kumar, H. Zhang, X. Liu, H. Gu, E. A. Stach, X. Liang, S. Liu, Z. Fakhraai, and D. Jariwala, "Giant gate-tunability of complex refractive index in semiconducting carbon nanotubes," ACS Photonics **7**, 2896–2905 (2020).
[39]Z. Li, S. Chen, J. Sun, X. Li, H. Qiu, and J. Yang, "Spatial and thickness dependence of coupling interaction of surface states and influence on transport and optical properties of few-layer Bi_2Se_3," J. Phys. **30**, 065503 (2018).
[40]H. Gu, B. Song, M. Fang, Y. Hong, X. Chen, H. Jiang, W. Ren, and S. Liu, "Layer-dependent dielectric and optical properties of centimeter-scale 2D WSe_2: Evolution from a single layer to few layers," Nanoscale **11**, 22762–22771 (2019).